A New High-Resolution Remote Sensing Monitoring Method for Nutrients in Coastal Waters

Jingjing Huang, Difeng Wang, Shuping Pan, Hongzhe Li, Fang Gong, Haoyan Hu, Xianqiang He, Yan Bai, and Zhuoqi Zheng

Abstract— Mariculture is an important offshore economic activity, and excessive farming can lead to the deterioration of sea ecology. The concentration of nutrients [mainly dissolved inorganic nitrogen (DIN) and orthophosphate-phosphorous (PO4)] is the main factor characterizing the health condition of farmed seas. Conventional field monitoring methods are spatiotemporally limited, and remote sensing technology has the advantages of high spatial coverage and long time series monitoring. Thus, the Sentinel-3 reflectance data and the in situ measured data for the offshore waters of Wenzhou were matched simultaneously. Then, the matched dataset between the Sentinel-2 band and the in situ measured data were obtained through spectral correspondence conversion between Sentinel-2 and Sentinel-3, and a machine learning algorithm was used to build the inversion model with an independent validation process. The correlations between the concentration of nutrients, area of rafts, and precipitation were assessed, and a strong positive correlation was found between the concentration of nutrients and the area of rafts, and a weak negative correlation was found between the former and precipitation.

Index Terms— Environmental monitoring of nori culture, Gaussian regression machine algorithm, nutrients, remote sensing monitoring, support vector machine (SVM).

I. INTRODUCTION

CHINA is the world's most advanced country in terms of mariculture based on area and total production [1], [2]. The mariculture area includes inshore netting, deep-water netting, cages, rafts, and bottom-seeded aquaculture, among other types. Mariculture generates revenue but also pollutes the sea, and unreasonable and unplanned aquaculture expansion will lead to the deterioration of the ocean's ecological environment, especially with increasing nutrient concentrations [3]. To prevent the ecological crisis caused by mariculture, we need to monitor the water quality of aquaculture areas dynamically.

Conventional monitoring of water quality factors, generally through navigation, buoys, offshore monitoring station sampling, or field measurements, provide accurate data; however, the cost is high, and it is difficult to achieve a large range of spatial measurements. Satellite remote sensing has the advantages of synchronous observation of large areas and dynamic and long-term observations, and the cost is relatively low [4], [5], [6].

To study the impact of mariculture on water quality, scholars previously used field sampling and analysis of farming areas. After data accumulation, some scholars used data from public sources, such as the statistical bulletin yearbook. Xiong et al. [7] and Xiao et al. [8] combined published literature data and data collected in their studies to quantify the amount of nutrients that can be removed by seaweed aquaculture, revealing that 1 ha of seaweed farming reduces nutrient inputs equivalent to 17.8 ha of nitrogen and 126.7 ha of phosphorus in China's coastal waters. In addition, Racine et al. [3], Wu et al. [9], Kim et al. [10], and He et al. [11] also evaluated the ability of seaweed aquaculture to remove nutrients from water bodies by conducting experiments, which demonstrated that biosorption has greater economic and environmental benefits than industrial absorption. In recent years, the development of remote sensing technology has also played a key role in water quality monitoring of marine waters, and more mature water quality monitoring includes chlorophyll a, suspended matter, and so on [12], [13]. These optically active water parameters have clear optical response characteristics [6]. Nutrients that do not have optically active components are generally established by empirical algorithms, which are relatively simple to construct and implement [14], [15]. Chang et al. [16], Liu et al. [17], Yu et al. [18], and Yuan et al. [19] used different algorithms to invert nutrient concentrations in different areas. Their study used different satellite data, such as MODIS, Landsat8, HJ-1, and other satellites, to monitor dissolved nonoptically active components, including total phosphorus, total inorganic nitrogen, nitrate, and total nitrogen, using direct and indirect
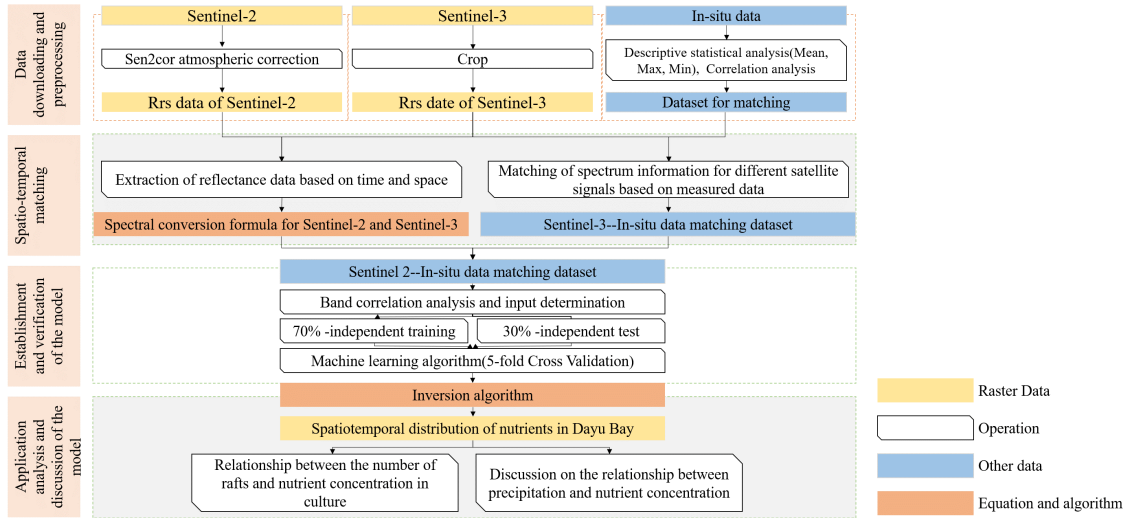
Fig. 1. Framework for assessing nutrient concentrations in Dayu Bay using remote sensing technology.
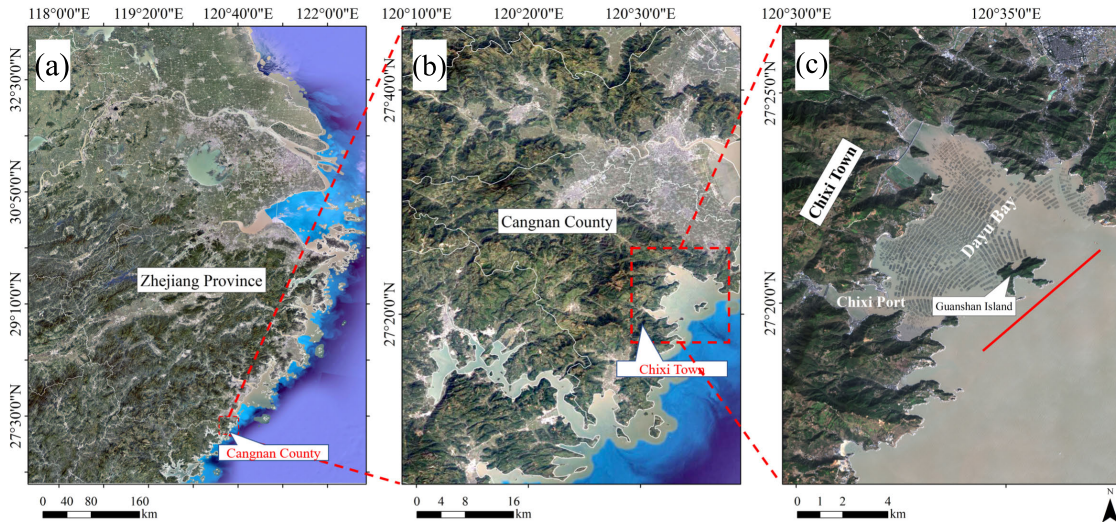

Fig. 2. Geographical location of the study area [(a) Cangnan County in Zhejiang Province. (b) Dayu Bay in Cangnan County. (c) Dayu Bay real color image. Regional variation was studied according to the average value on the red line in (c)].

methods. Machine learning algorithms, such as random forest, and genetic planning models were used to improve the inversion accuracy. However, remote sensing monitoring of marine nutrients uses mostly medium-spatial resolution satellite data, with less use of high-spatial-resolution data and a relative lack of mariculture area monitoring.

The Sentinel-2 satellite has a high spatial resolution and provides clear surface images, while the Sentinel-3 satellite has a high temporal resolution and frequent revisits over the same areas. In this article, we integrate the advantages of the dual satellites by first downloading L1-level Sentinel-2 images and preprocessing them with atmospheric correction and then selecting Sentinel-3 satellite images with the same date and area coverage to process and establish a map of the spectral correspondence between the dual satellites. Next, the Sentinel-3 data are matched with the measured data, and the matched dataset is mapped with Sentinel-2 images to obtain the modeling dataset, which is nearly ten times

larger than the dataset of direct matches with Sentinel-2; thus, the data will be more representative. Based on the machine learning algorithm, which has advantages in nonlinear regression fitting, an algorithm for nutrients in Dayu Bay is built. Based on this algorithm, a discussion of the spatial and temporal distribution characteristics of the aquaculture scale and water quality of the aquaculture area in Dayu Bay is provided, and the relationship between aquaculture quantity and the spatial-temporal distribution of nutrients is explored. The research framework is shown in Fig. 1.

II. MATERIALS AND METHODOLOGY

A. Study Area

Dayu Bay is located between 120.49°E and 120.65°E and 27.29°N and 27.42°N (see Fig. 2). The sea area of 46.98 km^2 is one of the five major bays in Wenzhou, the largest marine aquaculture area in Cangnan County, and one of the largest
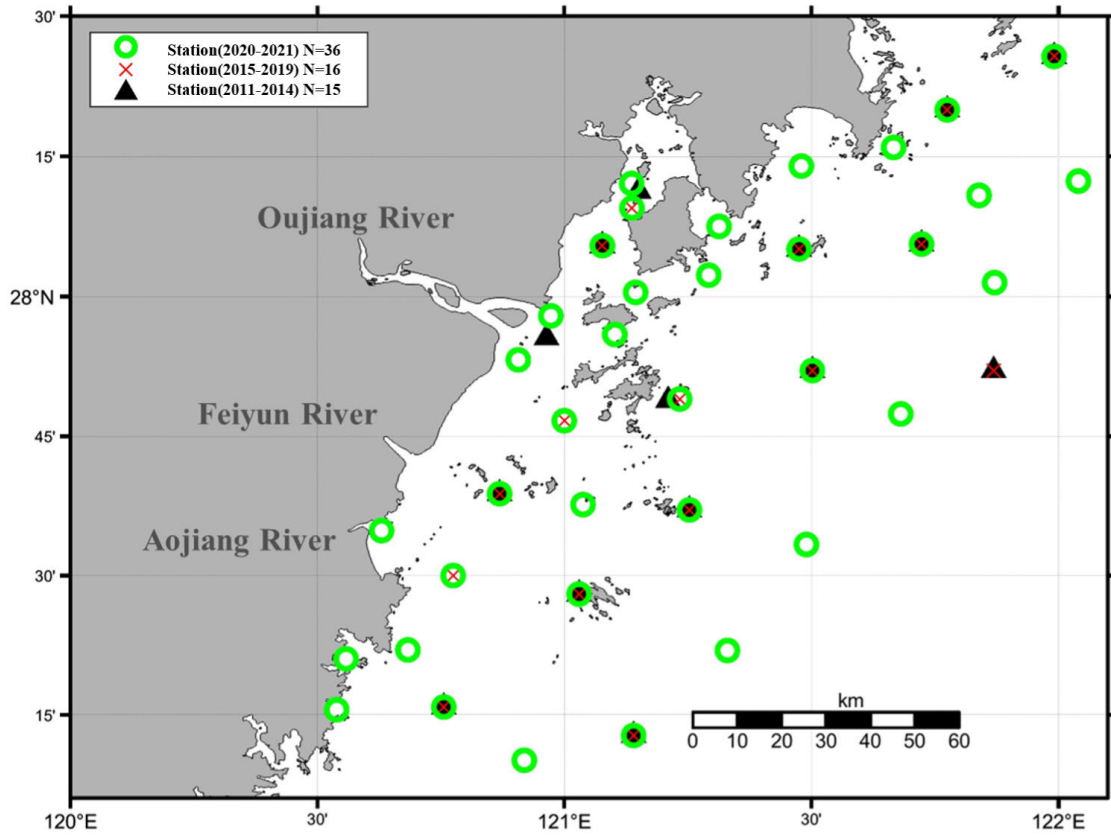
Fig. 3. Distribution of the measurement stations.

natural seaweed farms in China [20]. The bay shoreline is winding, and the mouth of the bay is home to the large island of Guanshan, as well as other islands that form a barrier. The winds are calm, the waves are relatively small, there are large streams that empty into the bay, and the water is nutrient-rich and suitable for shallow aquaculture (mainly seaweed and green crabs). In recent years, the scale of seaweed farming has grown rapidly, the density of farming has increased, and the economic value created has also increased on a yearly basis. To promote a win-win situation of providing economic benefits and protecting the ecological environment, monitoring the ecological environment of Dayu Bay is also important.

B. Satellite Data

The series of Sentinel satellites is dedicated to the space segment of the European Copernicus Program (GSC). Sentinel-3 is a global ocean and land monitoring satellite that is mainly used for global monitoring of the land, ocean, and atmospheric environment with a spatial resolution of 300 m [21]. The Ocean and Land Color Instrument (OLCI) onboard Sentinel-3 has 21 bands. Sentinel-2 is a high-resolution multispectral imaging satellite carrying a MultiSpectral Instrument (MSI) divided into two satellites, 2A and 2B, with a revisit period of ten days for one satellite and five days for two satellites [22]. The tile identifier of Sentinel-2 covering Dayu Bay is 51RTL, which acquired a total of 138 images with less than 50% cloud coverage from 2015 to 2022, is subject to rainy cloud coverage images in the summer, and the amount of available remote sensing images data is greater in autumn and winter

(see annual and seasonal distributions of Sentinel-2 data in Table AI in the Appendix for specific dates).

C. In Situ-Measured Data

The in situ measurement data cover the 2011–2021 period, with only 15 stations in Wenzhou waters during 2011–2015, 16 stations in 2016–2019, and 36 in 2020–2021. The specific station distribution is shown in Fig. 3. The measured values covered the concentrations of dissolved inorganic nitrogen C_{DIN} and orthophosphate-phosphorous C_{PO4}. The actual measurements had the advantage of high accuracy but were limited by the disadvantages of discrete stations, a noncontinuous time distribution, and the presence of only one station in Dayu Bay, which could not reflect the nutrient distribution; however, remote sensing could compensate for this disadvantage and fill in the missing data gaps.

D. Machine Learning-Based Supervised Classification Method to Identify Rafts

The spectral signatures of raft frames and water are different. First, to exclude the interference of multisource signals on land, water, and land separation was performed according to the water body index modified normalized difference water index (MNDWI) [23]. The formula of the MNDWI is shown in (1). When MNDWI > 0, the feature is identified as a water body, and when MNDWI < 0, the land is masked

$$\text{MNDWI} = (\text{BAND}_{\text{SWIR}} - \text{BAND}_{\text{Green}})$$
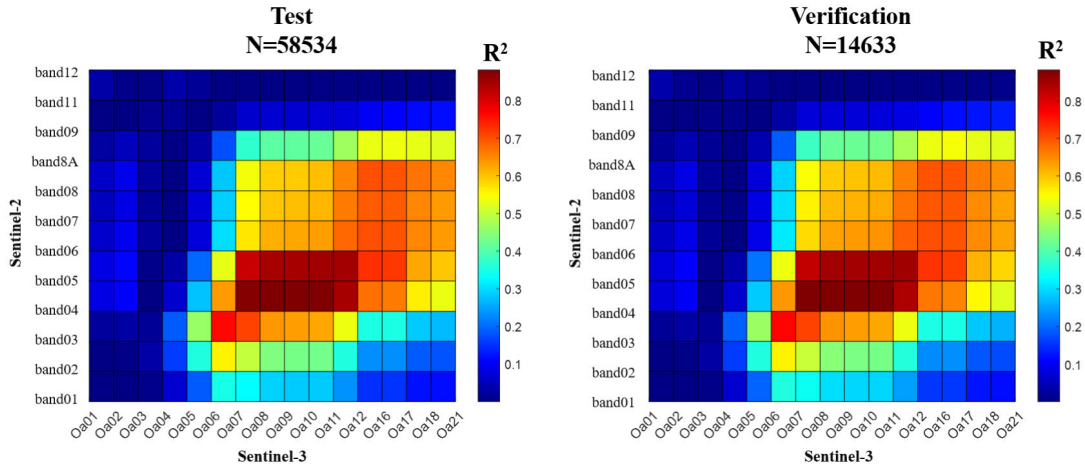$$/(\text{BAND}_{\text{SWIR}} + \text{BAND}_{\text{Green}}). \quad (1)$$

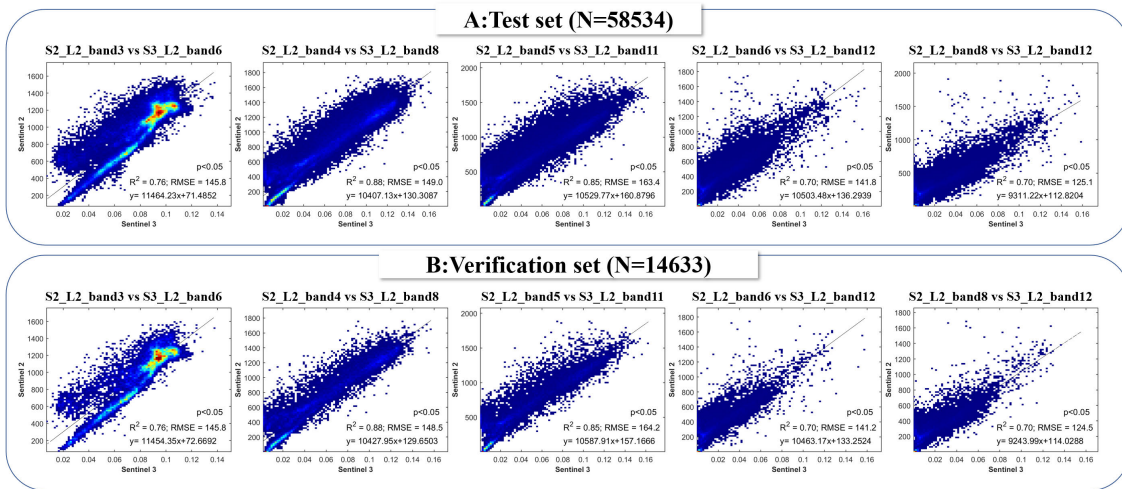Fig. 4. Heatmap of the correlation between different wavebands.

Fig. 5. Scatter plot of the spectral relationship between Sentinel-2 and Sentinel-3. (a) Test set ($N = 58\,534$). (b) Verification set ($N = 14\,633$).

The MNDWI images could distinguish between land and water, and the MNDWI values of raft shelves and seawater also had large differences. To further extract raft shelves, the images were cropped to the minimum study area. Taking the MNDWI thresholds of 0.3 and 0.7, raft shelves and highly turbid water bodies were easily misclassified, and the manually supervised machine learning algorithm based on the classification results could be optimized and corrected by manual recognition.

E. Spectral Response of Sentinel-3 and Sentinel-2

Sentinel-3 data were derived from atmospherically corrected surface reflectance data with a spatial resolution of 300 m, while Sentinel-2 downloaded L1-level data, using sen2cor for atmospheric correction [24]. The data of Sentinel-2 and 3 from the same day were selected for a total of 18 days (see Table AII in the appendix for specific dates), and to ensure that both datasets had the same spatial resolution, the Sentinel-2 data were resampled using the nearest neighbor method. In total, 73 167 valid matching points were obtained, and the matched data were divided into test and validation sets. Since the two satellites have different band settings and the

central wavelengths are not exactly the same, the correlation between all bands was determined, which is shown in Fig. 4.

The bands with correlation coefficients (R^2) greater than 0.70 were retained, and the bands with similar central wavelengths were finally selected. Bands $b3$, $b4$, $b5$, $b6$, and $b8$ of Sentinel-2 corresponded to bands $b6$, $b8$, $b11$, $b12$, and $b12$ of Sentinel-3, respectively; the central wavelengths corresponded to 560, 665, 705, 740, and 842 nm; and the spectral data were matched.

The mapped scatter plot is shown in Fig. 5(a). The five bands ($b3$, $b4$, $b5$, $b6$, and $b8$) of Sentinel-2 were highly correlated with those of Sentinel-3, and, thus, the spectrum of Sentinel-3 could be mapped to Sentinel-2 by a linear relationship.

Sentinel-3 and 2 images from another day were selected to validate the map relationships obtained above. The results are shown in Fig. 5(b). The validation accuracy was high, and the mapping relationship was stable.

F. Model Construction and Selection

When matching the actual data with the remote sensing data of Sentinel-2 and Sentinel-3, we obtained only ten sets
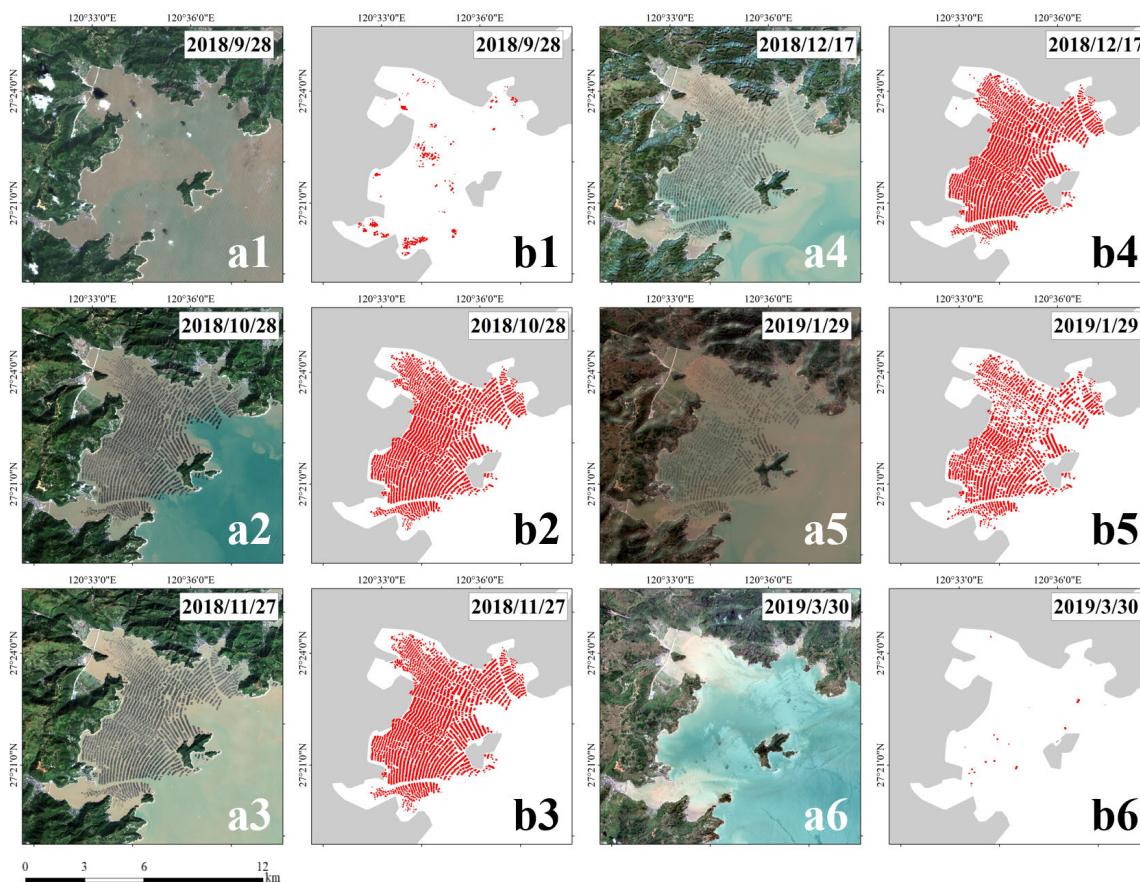
Fig. 6. True-color remote sensing image and raft frame extraction results of Dayu Bay. (a1)–(a6) True color images. (b1)–(b6) Results of raft extraction.

TABLE I
STATISTICS OF MATCHED DATA

	Amount of data	Mean (mg/L)	Maximum (mg/L)	Minimum (mg/L)
DIN	112	0.312	1.154	0.002
PO4	112	0.022	0.071	0.001

of effective matched data for Sentinel-2 and 112 sets for Sentinel-3 in the offshore waters of Wenzhou. The two-day reentry date of Sentinel-3 greatly increased the amount of matched data. Statistical modeling datasets and the distribution of each measured water quality factor concentration are shown in Table I.

Based on the spectral correspondence between Sentinel-2 and Sentinel-3 (see Section II-E), the Sentinel-3 reflectance response matching that of Sentinel-2 was developed and modeled based on various machine learning algorithms.

Support vector machine (SVM) was first proposed in 1964. SVM is a sparse and robust classifier that uses a hinge loss function to calculate empirical risk and adds a regularization term to the solution system to optimize structural risk [25]. SVM can perform nonlinear classification by kernel methods and is one of the common kernel learning methods [26], [27]. SVM models are supported by rigorous mathematical theory, are highly interpretable, and do not rely on statistical methods, thus simplifying the usual classification and regression problems. They can identify key samples and support principal component analysis; the use of kernel functions can allow nonlinear regression problems to be addressed and are suitable for regression operations on small sample datasets [28], [29].

The Gaussian process regression (GPR) model is a nonparametric kernel probability model with a finite set of multivariate distributed random variables. Each linear combination is uniformly distributed. The Gaussian process is named after Carl Friedrich Gauss, as it is based on the Gaussian distribution, which is an infinite dimensional extension of the multivariate normal distribution. Gaussian processes are used for statistical modeling, regression to multiple objective values, and mapping in high-dimensional analysis. Gaussian models include Matern 5/2 GPR, exponential GPR, rational quadratic GPR, and squared exponential GPR [30].
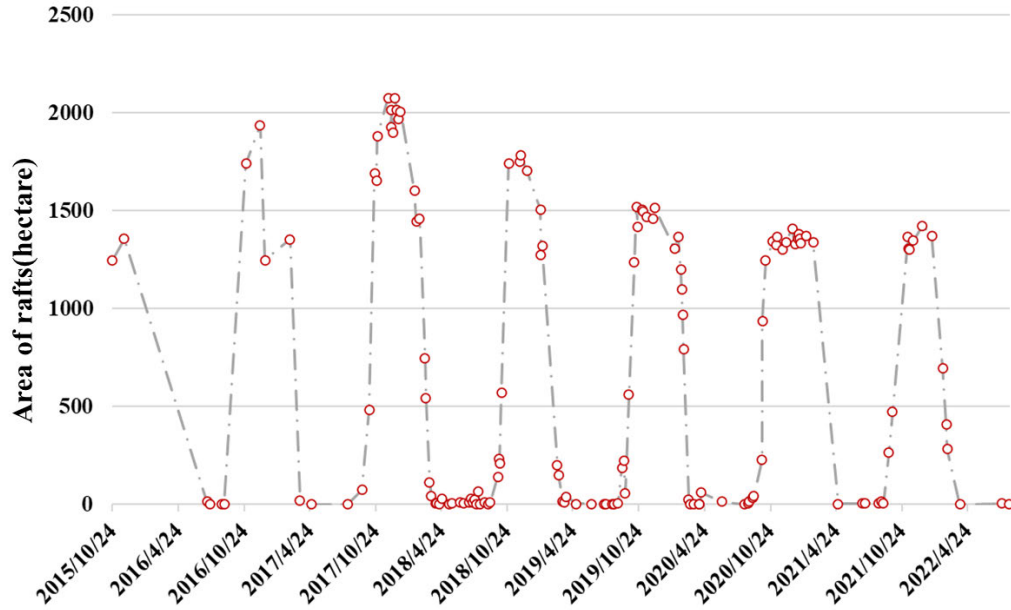
Fig. 7.   Graph of changes in the area of rafts.

TABLE II
SINGLE-BAND CORRELATION OF MEASURED DIN AND PO4 WITH SENTINEL-2 DATA

R^2	B3	B4	B5	B6	B8
PO4	0.20	0.28	0.22	0.10	0.22
DIN	0.24	0.38	0.34	0.20	0.34

III. RESULTS

A. Identification Results for Breeding Raft Frames

According to the extraction method for farming rafts presented in Section II-D, the area of rafts in different periods in Dayu Bay from 2015 to 2022 was obtained, and the extraction results are shown in Fig. 6.

The identification results correspond to the culture cycle of nori [31]. Usually, rafts appeared at the end of September-early October of each year and disappeared by the end of March of the following year, and there were no rafts from April to August. From 2015 to 2022 (see Fig. 7), the overall area of rafts showed a decreasing trend on a yearly basis, with the peak occurring on November 27, 2017, when the statistical area reached a maximum of 2076.96 ha, and after 2019, the farmed area was below 1500 ha.

B. Accuracy of the Water Quality Algorithm

The modeling dataset was analyzed to calculate the correlation between the measured DIN, PO4, and five bands and to try multiple band combination forms to obtain the best input signal for modeling. The single-band correlations are shown in Table II.

As seen in the above table, the correlation between the measured nutrients and single bands was low, and attempts were made to improve the correlation in the form of band combinations. Band combination included using multiple bands directly as input, as well as creating different combinations between bands before using them as input (see results in Table III).

The correlation with the measured nutrients could be improved by combining the bands as inputs. The strongest correlations with measured nutrients were found for the combination of the wave ratio $X1$ form: $B3/B4$ and $B8/B5$, which were comparable to the $X8$ form in which each of the five bands was used as an independent input, so these two forms were used as inputs to the machine learning model.

The modeling dataset was divided into modeling and validation sets according to the ratios of 80% and 20%, and fivefold cross-validation was implemented to prevent overfitting. Attempts were made based on multiple models, and the results are shown in Table IV.

The SVM model algorithm, based on the quadratic kernel function (quadratic SVM), performed best for C_{DIN}, with R^2 reaching 0.67 for the modeling set and 0.69 for the validation set. The GPR model, based on the exponential kernel function (exponential GPR), performed best for C_{PO4}, with R^2 reaching 0.97 for the modeling set and 0.6 for the validation set. The scatter plots of both models are shown in Fig. 8. The inversion results were close to the 1:1 line.

TABLE III

STATISTICAL ANALYSIS OF THE CORRELATION BETWEEN MULTIPLE BAND COMBINATIONS AND MEASURED NUTRIENTS (BRIEF VERSION:
$X1$–$X8$ REPRESENT THE FORMS OF BAND COMBINATION; BX AND BY REPRESENT DIFFERENT BANDS OF SENTINEL-2)

Band combination form	DIN	PO4
X1=BX/BY	X=3，Y=4,R^2=0.45	X=8，Y=5,R^2=0.34
X2=(log10(BX)+log10(BY))/(log10(BX)/log10(BY))	X=3，Y=4,R^2=0.5	X=3，Y=4,R^2=0.38
X3=(log10(BX)-log10(BY))/(log10(BX)/log10(BY))	X=4，Y=3,R^2=0.46	X=5，Y=8,R^2=0.34
X4=(log10(BX)-log10(BY))/(log10(BX)+log10(BY))	X=3，Y=4,R^2=0.49	X=3，Y=4,R^2=0.34
X5=log10(BX)/log10(BY)	X=3，Y=4,R^2=0.49	X=3，Y=4,R^2=0.35
X6=log10(BX/BY)	X=3，Y=4,R^2=0.46	X=8，Y=5,R^2=0.34
X7=log10(BX+BY)	X=4，Y=5,R^2=0.47	X=4，Y=5,R^2=0.35
X8=B3,B4,B5,B6,B8	R^2=0.46	R^2=0.43

TABLE IV

ACCURACY EVALUATION OF DIFFERENT MODELING SETS AND VALIDATION SETS

Output	Input	Model	Training Set		Test Set	
			R2	RMSE	R2	RMSE
DIN	B3,B4,B5,B6,B8	Quadratic SVM	0.67	0.144	0.69	0.133
		Medium Gaussian SVM	0.58	0.161	0.66	0.138
	(log10(B3)+log10(B4))/(log10(B3)/log10(B4))	Squared Exponential GPR	0.54	0.169	0.68	0.134
	B3/B4,B8/B4	Squared Exponential GPR	0.56	0.166	0.70	0.130
PO4	(log10(B3)+log10(B4))/(log10(B3)/log10(B4))	Medium Gaussian SVM	0.47	0.015	0.49	0.015
	B3/B4,B8/B4	Squared Exponential GPR	0.54	0.013	0.64	0.012
	B3,B4,B5,B6,B8	Exponential GPR	0.97	0.003	0.60	0.013

C. Results of the Spatial and Temporal Distributions of Nutrients

Overall, the average C_{DIN} in Dayu Bay was 0.41 mg/L and the average C_{PO4} was 0.033 mg/L during the nearly eight-year period from 2015 to 2022.

Regarding the spatial distribution of nutrients in Dayu Bay (see Fig. 9), the inner bay had higher nutrient levels than the outer bay, and the northern corner was influenced by river input from Chixi town and sediment siltation, so the concentration of nutrients was high; the southwest corner had river input from Chixi town, so it was also a source of nutrients, and the concentration of nutrients in Chixi port was also high [the locations of Chixi town and Chixi port are marked in Fig. 2(c)]. To explore the seasonal characteristics of nutrients in Dayu Bay, the average nutrient concentration was statistically analyzed for different seasons. This article considers March to May to be spring, June to August to be summer, September to November to be autumn, and December to February of the following year to be winter. There was little spatial difference in nutrients in winter compared with summer, especially in the bay filled with a large area of breeding rafts, where the mobility of the water body was reduced, the river input into the winter was lower than the input in the summer, the flow speed was slower, the scouring was poorer, and the accumulation of high nutrient concentrations in the estuary was weakened.

To avoid the interference of rafts, the nutrient concentrations in the outer bay were monitored over a long time series from 2015 to 2022 (see Fig. 2). To further avoid the interference of rafts, a monitoring line was established in the outer bay (see Fig. 10), and the mean value on the line was used to characterize the trend of nutrient changes in Dayu Bay in the long time series. Between 2015 and 2022, C_{DIN} and C_{PO4} showed oscillating fluctuations, with the highest C_{DIN} occurring on October 21, 2017, with a concentration of 0.76 mg/L, and the lowest value occurring on August 4, 2018, with a concentration of 0.15 mg/L; the highest value of C_{PO4} also occurred on October 21, 2017, with a concentration
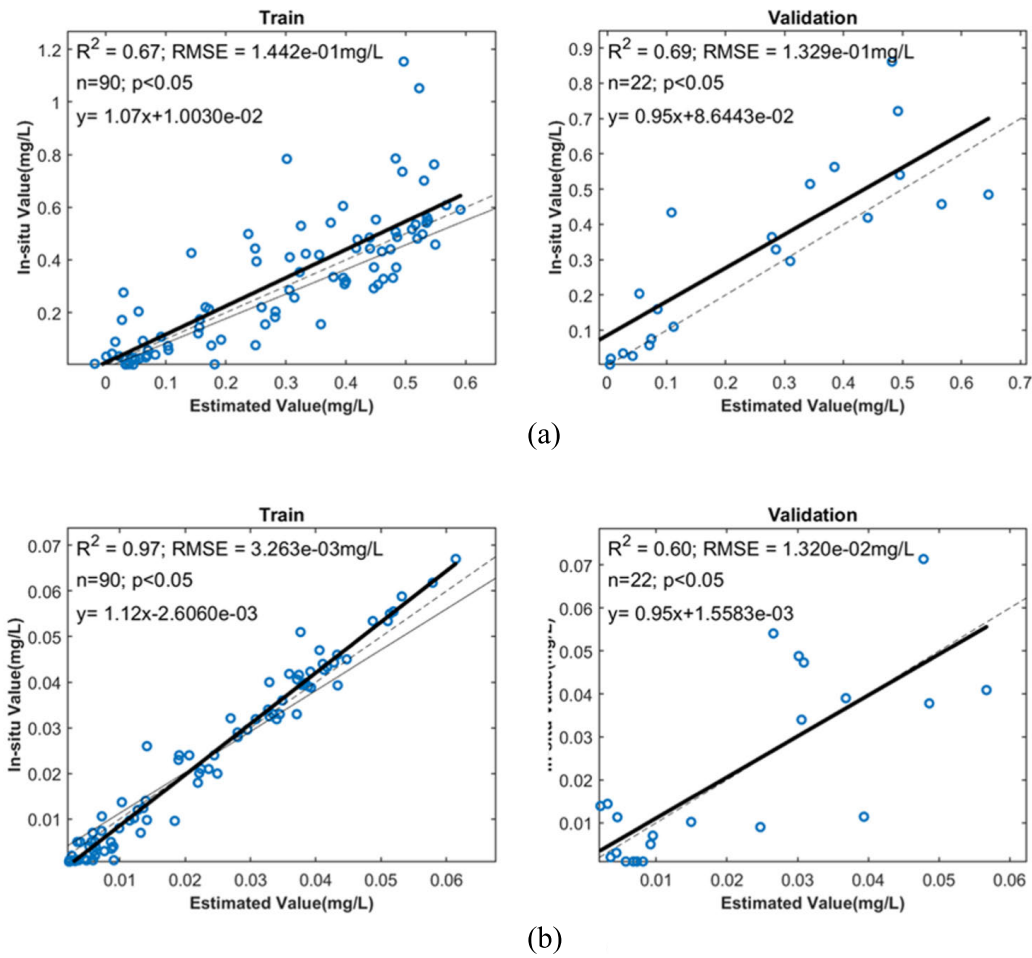
Fig. 8.   (a) Accuracy of the C_DIN model. (b) Accuracy of the C_PO4 model.
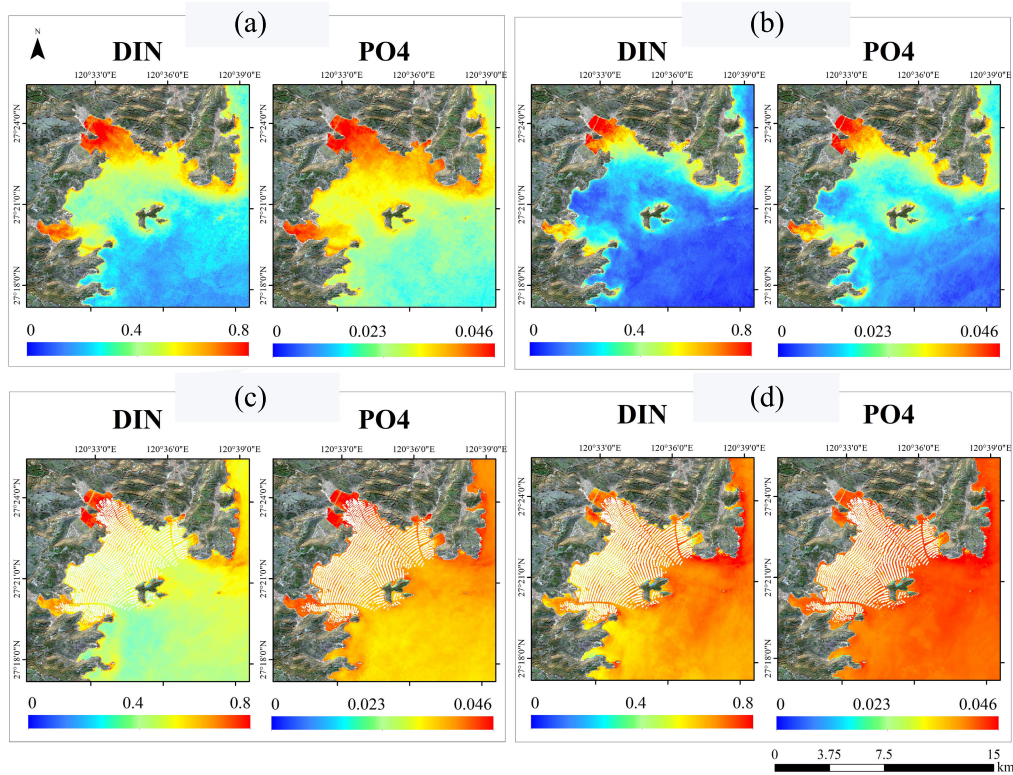
Fig. 9.   Spatial distribution characteristics of remote sensing monitoring of nutrients in Dayu Bay [(a) Spring. (b) Summer. (c) Autumn. (d) Winter. The locations of Chixi town and Chixi port are marked in Fig. 2(c)].
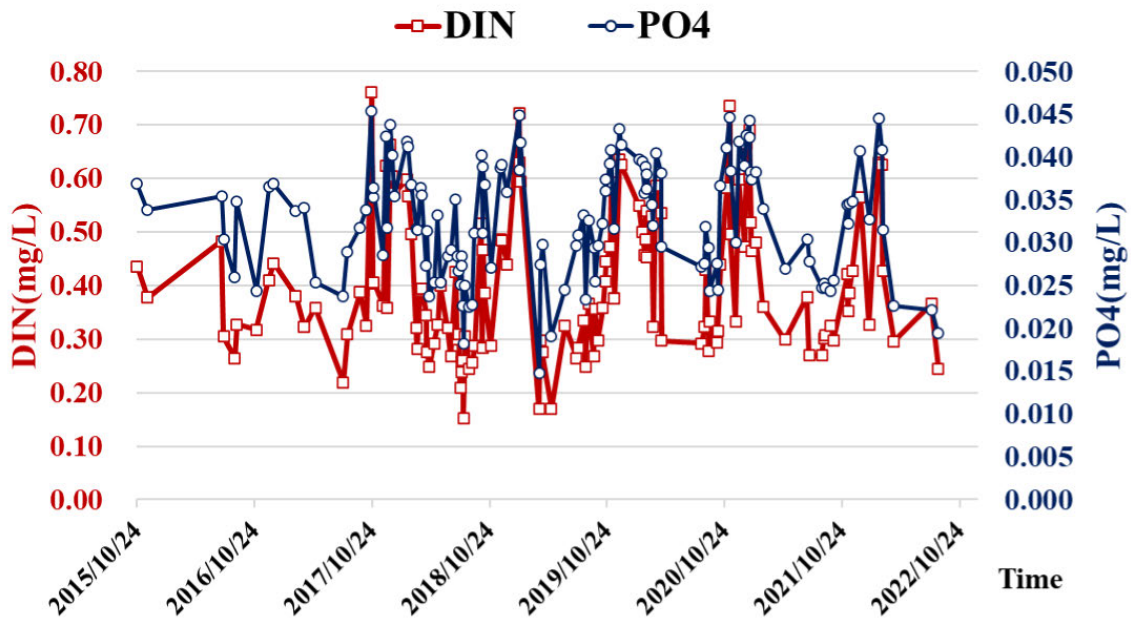
Fig. 10. Long time series monitoring results of nutrients in Dayu Bay.
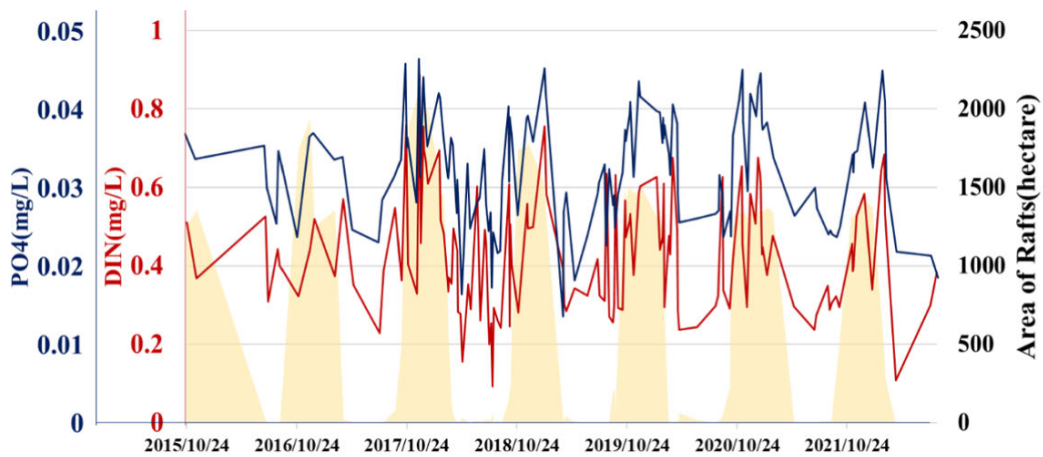
Fig. 11. Statistical plot of the nutrient concentration and area of rafts.
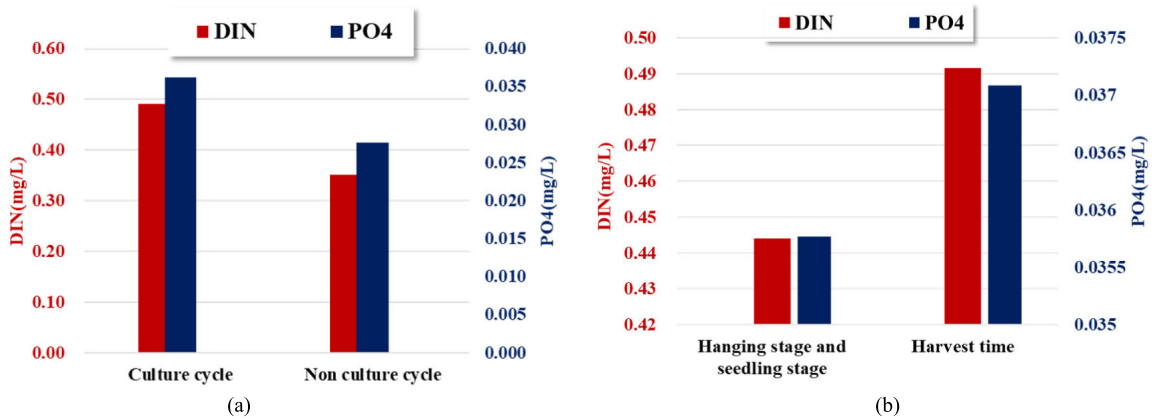
Fig. 12. (a) Comparison of nutrient concentrations in the culture cycle and nonculture cycle. (b) Comparison of nutrient concentrations during the netting, seeding, and harvesting periods.

Fig. 13.   Average monthly nutrients, area of culture rafts, and rainfall data (2015–2022).

Fig. 14.   Scatterplot of monthly average nutrient concentrations versus the area of rafts and rainfall.

of 0.045 mg/L, and the lowest value occurred on March 17, 2019, with a concentration of 0.015 mg/L. The C_{DIN} and C_{PO4} of Dayu Bay varied significantly within seasons during the last eight years, with peak nutrient concentrations occurring in approximately October–November and with less variation between years.
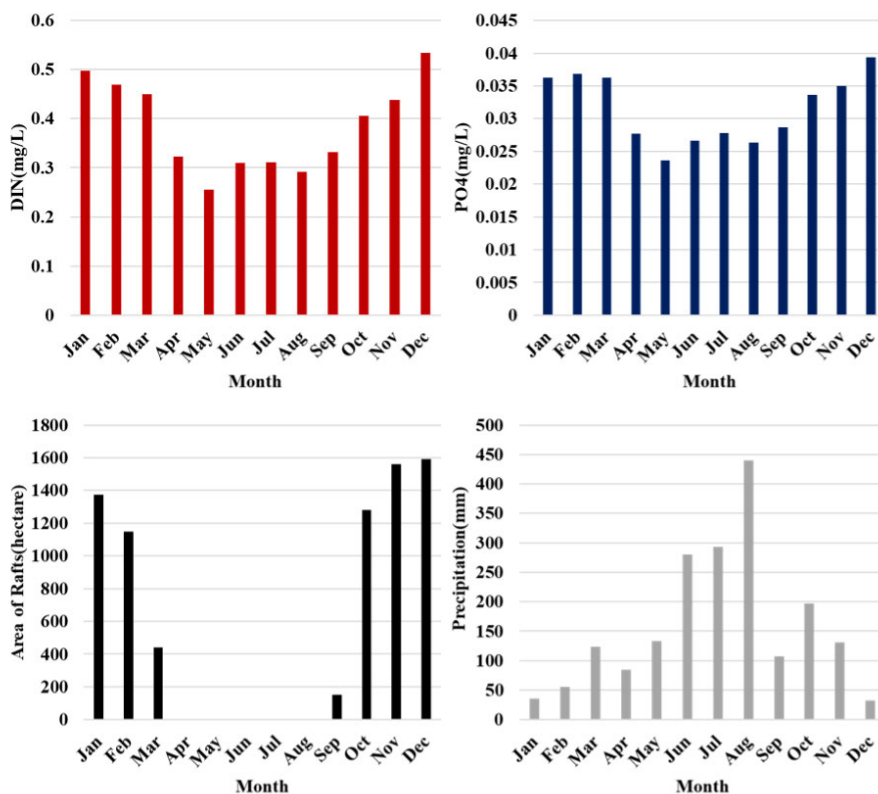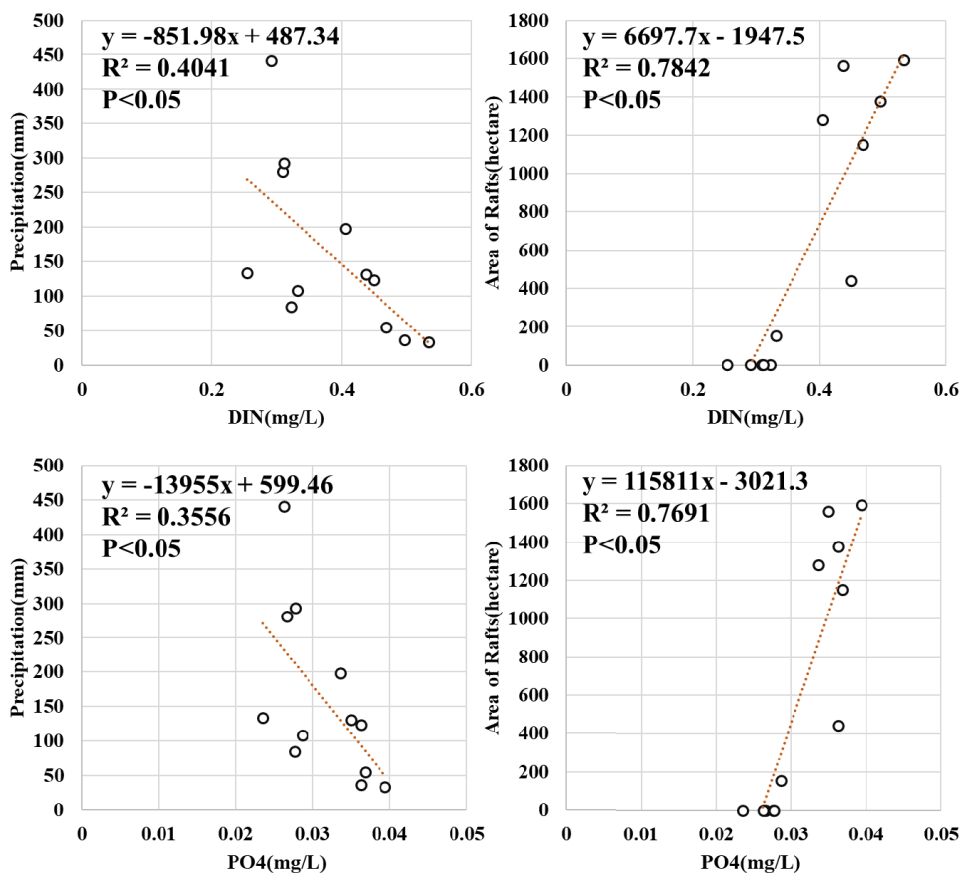
IV. DISCUSSION

A. Exploration of the Relationship Between Nutrient Concentrations Changes and the Culture Cycle

According to the raft area statistics described in Section III-A, the area of rafts in autumn 2017 was the highest in recent years, which coincided with the year in which the highest nutrient concentrations occurred (see Fig. 11). In the same way, within a year, the months with elevated nutrient corresponded to the culture cycle (approximately October = March of the following year).

Statistical comparison of nutrients during the culture cycle and nonculture periods showed that nutrient concentrations were higher during the culture cycle than during the nonculture cycle, with C_{DIN} being approximately 1.5 times higher and C_{PO4} being approximately 1.29 times higher during the culture period than during the nonculture period. However, there was also a seasonal effect.

In the culture cycle [see Fig. 12(b)], the average concentration of nutrients also differed between October and early December of each year, when the netting and seeding periods were used for nori culture, and between late December and early April of the following year, when the harvest period occurred. The concentration of nutrients was lower in the netting and seedling stages than in the harvesting stage, where the C_{DIN} in the harvesting stage was approximately 10% higher than that in the netting and seedling stages, and the C_{PO4} was more similar.

During harvest, there are multiple reasons why nutrient concentrations may be higher. One of the main factors is the vigorous growth and dense population of laver. As laver grows rapidly, some parts of it become overgrown and eventually rot, falling off into the seawater. This process releases nitrogen into the water, which can contribute to increased nutrient levels [32]. In addition, farmers may choose to add nitrogen- and phosphorus-containing nutrients to the aquaculture area during the harvesting process. However, the use of such fertilizer can also lead to an increase in nitrate and phosphate concentrations in seawater, further contributing to higher nutrient levels [33]. Overall, these multiple factors can result in higher nutrient levels during the laver harvest season.

B. Discussion of the Mechanism Influencing Nutritional Change

For coastal bays, nutrient sources are described as follows: 1) land-based rivers; 2) atmospheric deposition; 3) benthic sediments; 4) submarine groundwater discharge; and 5) mariculture [34]. This study focused on precipitation driving atmospheric deposition and mariculture in Dayu Bay. The month-by-month precipitation data of Wenzhou City were

obtained and averaged on a monthly basis, while the same calculations were performed for the nutrient concentrations and the area of raft culture, as shown in Fig. 13.

According to the statistical results, the nutrient in Dayu Bay showed significant seasonal characteristics that mainly manifested as lower concentrations in late spring and summer and high concentrations in winter; the seasonality of raft rack culture corresponds to the culture cycle of nori, and the quantity reaches the maximum in December; the rainfall in Wenzhou was mainly concentrated in the summer (June–August), and the average monthly precipitation was above 250 mm. The correlations between the monthly average nutrient and the area of rafts and rainfall were calculated from the statistical results. Fig. 14 shows that the overall nutrient concentration was positively correlated with the area of culture rafts and negatively correlated with rainfall, and the correlation with the area of culture rafts was stronger than that with rainfall.

V. CONCLUSION

In this article, the representation of the matched dataset was improved by using the two satellites, and a highly accurate nutrient inversion model was obtained through experiment. Thus, the nutrient inversion model provides support for future similar studies in offshore waters and provides an example for monitoring the quality of aquaculture waters. Based on the advantages of the Sentinel-2 and Sentinel-3 satellites, this article draws the following conclusions through experiments:

1) We integrated the advantages of the dual satellites (Sentinel-2 and Sentinel-3). Sentinel-2 had a high spatial resolution, and the two-day reentry date of Sentinel-3 greatly increased the amount of matched data, which made the matching dataset more representative. Remote sensing monitoring of the inversion model was obtained through various machine learning algorithms. Finally, the R^2 of the C_{DIN} model reached 0.60, and the R^2 of C_{PO4} was 0.58 with high accuracy, indicating high applicability.

2) Based on the above information, the spatial and temporal changes of nutrients in Dayu Bay were monitored, and the area of rafts in this sea area gradually decreased from 2015 to 2022. The concentrations of nutrients showed a fluctuating trend, with significant seasonal characteristics and small interannual changes, and the changes were relatively slow in the last eight years.

3) Combined with the culture cycle of nori, the concentrations of nutrient in the culture cycle were much higher than that in the nonculture period. During the culture cycle, C_{DIN} was approximately 10% higher in the harvesting period from late December to April than in the hanging and seeding periods from October to early December, and C_{PO4} was more similar. Analysis of the combined precipitation data showed that nutrient concentrations in Dayu Bay were negatively correlated with precipitation and more positively correlated with the area of culture rafts.

APPENDIX

TABLE AI

ANNUAL AND SEASONAL DISTRIBUTIONS OF SENTINEL-2 DATA [SPRING (MARCH–MAY), SUMMER (JUNE–AUGUST), AUTUMN (SEPTEMBER–NOVEMBER), AND WINTER (DECEMBER–FEBRUARY)]

Year	Spring	Summer	Autumn	Winter
2015			2	3
2016		3	1	10
2017	2	2	6	3
2018	10	8	9	8
2019	5	6	11	9
2020	5	4	10	5
2021	2	4	7	
2022	1	2		
Total	25	29	46	38

TABLE AII

DATES OF REMOTE SENSING IMAGES USED FOR SENTINEL 2 AND SENTINEL 3 SPECTRAL RESPONSES ($n = 18$)

Year	2018	2019	2020	2021	2022
Date	2018/4/9	2019/4/1	2020/1/31	2021/1/15	2022/2/10
	2018/7/25	2019/11/2	2020/2/5	2021/2/19	2022/5/5
	2018/10/3	2019/12/7	2020/4/8	2021/4/30	
	2018/10/18	2019/12/12	2020/8/18	2021/9/27	

TABLE AIII

STATISTICAL ANALYSIS OF THE CORRELATION BETWEEN MULTIPLE BAND COMBINATIONS AND MEASURED NUTRIENTS (COMPLETE EDITION)

DIN						PO4					
X1=BX/BY											
X \ Y	b3	b4	b5	b6	b8	X \ Y	b3	b4	b5	b6	b8
b3		0.45	0.31	0.11	0.36	b3		0.33	0.20	0.05	0.24
b4	0.43		0.01	0.07	0.05	b4	0.29		0.03	0.12	0.01
b5	0.27	0.02		0.11	0.43	b5	0.15	0.05		0.15	0.33
b6	0.08	0.08	0.11		0.20	b6	0.02	0.12	0.14		0.20
b8	0.33	0.04	0.45	0.19		b8	0.18	0.00	0.34	0.21	
X2=(log10(BX)+log10(BY))/(log10(BX)/log10(BY))											
X \ Y	b3	b4	b5	b6	b8	X \ Y	b3	b4	b5	b6	b8
b3		0.50	0.47	0.35	0.48	b3		0.38	0.33	0.20	0.33
b4	0.08		0.45	0.31	0.46	b4	0.07		0.31	0.17	0.32
b5	0.07	0.46		0.33	0.47	b5	0.07	0.36		0.20	0.34
b6	0.06	0.44	0.47		0.47	b6	0.08	0.37	0.36		0.36
b8	0.04	0.46	0.46	0.31		b8	0.05	0.36	0.33	0.18	

TABLE AIII
(Continued.) STATISTICAL ANALYSIS OF THE CORRELATION BETWEEN MULTIPLE BAND
COMBINATIONS AND MEASURED NUTRIENTS (COMPLETE EDITION)

X3=(log10(BX)-log10(BY))/(log10(BX)/log10(BY))

X\Y	b3	b4	b5	b6	b8	X\Y	b3	b4	b5	b6	b8
b3		0.45	0.29	0.08	0.34	b3		0.31	0.17	0.02	0.21
b4	0.46		0.01	0.09	0.04	b4	0.33		0.04	0.13	0.00
b5	0.31	0.01		0.12	0.45	b5	0.19	0.04		0.15	0.34
b6	0.11	0.07	0.11		0.19	b6	0.04	0.11	0.14		0.21
b8	0.37	0.05	0.44	0.20		b8	0.24	0.01	0.33	0.21	

X4=(log10(BX)-log10(BY))/(log10(BX)+log10(BY))

X\Y	b3	b4	b5	b6	b8	X\Y	b3	b4	b5	b6	b8
b3		0.49	0.34	0.15	0.42	b3		0.34	0.21	0.06	0.27
b4	0.49		0.01	0.03	0.13	b4	0.34		0.03	0.07	0.05
b5	0.34	0.01		0.04	0.44	b5	0.21	0.03		0.08	0.33
b6	0.15	0.03	0.04		0.16	b6	0.06	0.07	0.08		0.17
b8	0.42	0.13	0.44	0.16		b8	0.27	0.05	0.33	0.17	

X5=log10(BX)/log10(BY)

X\Y	b3	b4	b5	b6	b8	X\Y	b3	b4	b5	b6	b8
b3		0.49	0.34	0.15	0.42	b3		0.35	0.22	0.07	0.27
b4	0.49		0.01	0.03	0.13	b4	0.34		0.03	0.07	0.06
b5	0.34	0.01		0.04	0.43	b5	0.21	0.03		0.08	0.33
b6	0.14	0.03	0.04		0.16	b6	0.06	0.07	0.08		0.17
b8	0.41	0.13	0.44	0.15		b8	0.27	0.05	0.33	0.17	

X6=log10(BX/BY)

X\Y	b3	b4	b5	b6	b8	X\Y	b3	b4	b5	b6	b8
b3		0.46	0.30	0.10	0.36	b3		0.32	0.18	0.03	0.22
b4	0.46		0.01	0.08	0.04	b4	0.32		0.04	0.12	0.01
b5	0.30	0.01		0.11	0.44	b5	0.18	0.04		0.15	0.34
b6	0.10	0.08	0.11		0.20	b6	0.03	0.12	0.15		0.21
b8	0.36	0.04	0.44	0.20		b8	0.22	0.01	0.34	0.21	

X7=log10(BX+BY)

X\Y	b3	b4	b5	b6	b8	X\Y	b3	b4	b5	b6	b8
b3		0.38	0.38	0.34	0.37	b3		0.30	0.29	0.26	0.28
b4	0.38		0.47	0.46	0.47	b4	0.30		0.35	0.34	0.35
b5	0.38	0.47		0.45	0.47	b5	0.29	0.35		0.31	0.34
b6	0.34	0.46	0.45		0.45	b6	0.26	0.34	0.31		0.31
b8	0.37	0.47	0.47	0.45		b8	0.28	0.35	0.34	0.31	

X8=B3,B4,B5,B6,B8

0.46	0.43

REFERENCES

[1] J. Xu, L. Han, and W. Yin, "Research on the ecologicalization efficiency of mariculture industry in China and its influencing factors," *Mar. Policy*, vol. 137, Mar. 2022, Art. no. 104935, doi: 10.1016/j.marpol.2021.104935.

[2] X. Yu et al., "Submarine groundwater-derived inorganic and organic nutrients vs. mariculture discharge and river contributions in a typical mariculture bay," *J. Hydrol.*, vol. 613, Oct. 2022, Art. no. 128342, doi: 10.1016/j.jhydrol.2022.128342.

[3] P. Racine et al., "A case for seaweed aquaculture inclusion in U.S. nutrient pollution management," *Mar. Policy*, vol. 129, Jul. 2021, Art. no. 104506, doi: 10.1016/j.marpol.2021.104506.

[4] H. J. Jeong et al., "A hierarchy of conceptual models of red-tide generation: Nutrition, behavior, and biological interactions," *Harmful Algae*, vol. 47, pp. 97–115, Jul. 2015, doi: 10.1016/j.hal.2015.06.004.

[5] R. Lins, J.-M. Martinez, D. M. Marques, J. Cirilo, and C. Fragoso, "Assessment of chlorophyll—A remote sensing algorithms in a productive tropical estuarine-lagoon system," *Remote Sens.*, vol. 9, no. 6, p. 516, May 2017, doi: 10.3390/rs9060516.

[6] M. Saberioon, J. Brom, V. Nedbal, P. Souček, and P. Císař, "Chlorophyll—A and total suspended solids retrieval and mapping using sentinel-2A and machine learning for inland waters," *Ecolog. Indicators*, vol. 113, Jun. 2020, Art. no. 106236, doi: 10.1016/j.ecolind.2020.106236.

[7] Y. Xiong, L. Gao, L. Qu, J. Xu, Z. Ma, and G. Gao, "The contribution of fish and seaweed mariculture to the coastal fluxes of biogenic elements in two important aquaculture areas, China," *Sci. Total Environ.*, vol. 856, Jan. 2023, Art. no. 159056, doi: 10.1016/j.scitotenv.2022.159056.

[8] X. Xiao et al., "Nutrient removal from Chinese coastal waters by large-scale seaweed aquaculture," *Sci. Rep.*, vol. 7, no. 1, Apr. 2017, Art. no. 46613, doi: 10.1038/srep46613.

[9] J. Wu, S. W. Rogers, R. Schaumann, C. Higgins, and N. Price, "Bioextractive aquaculture as an alternative nutrient management strategy for water resource recovery facilities," *Water Res.*, vol. 212, Apr. 2022, Art. no. 118092, doi: 10.1016/j.watres.2022.118092.

[10] J. K. Kim, G. P. Kraemer, and C. Yarish, "Field scale evaluation of seaweed aquaculture as a nutrient bioextraction strategy in Long Island Sound and the Bronx River Estuary," *Aquaculture*, vol. 433, pp. 148–156, Sep. 2014, doi: 10.1016/j.aquaculture.2014.05.034.

[11] P. He et al., "Bioremediation efficiency in the removal of dissolved inorganic nutrients by the red seaweed, *Porphyra yezoensis*, cultivated in the open sea," *Water Res.*, vol. 42, nos. 4–5, pp. 1281–1289, Feb. 2008, doi: 10.1016/j.watres.2007.09.023.

[12] T. W. Cui et al., "Remote sensing of chlorophyll a concentration in turbid coastal waters based on a global optical water classification system," *ISPRS J. Photogramm. Remote Sens.*, vol. 163, pp. 187–201, May 2020, doi: 10.1016/j.isprsjprs.2020.02.017.

[13] Y. W. Kim et al., "Validity evaluation of a machine-learning model for chlorophyll a retrieval using Sentinel-2 from inland and coastal waters," *Ecolog. Indicators*, vol. 137, Apr. 2022, Art. no. 108737, doi: 10.1016/j.ecolind.2022.108737.

[14] D. Odermatt, A. Gitelson, V. E. Brando, and M. Schaepman, "Review of constituent retrieval in optically deep and complex waters from satellite imagery," *Remote Sens. Environ.*, vol. 118, pp. 116–126, Mar. 2012, doi: 10.1016/j.rse.2011.11.013.

[15] T. Platt, S. Sathyendranath, H. Bouman, C. Brockmann, and D. McKee, "Special issue on remote sensing of ocean color: Theory and applications," *Sensors*, vol. 20, no. 12, p. 3445, Jun. 2020, doi: 10.3390/s20123445.

[16] N.-B. Chang, Z. Xuan, and Y. J. Yang, "Exploring spatiotemporal patterns of phosphorus concentrations in a coastal bay with MODIS images and machine learning models," *Remote Sens. Environ.*, vol. 134, pp. 100–110, Jul. 2013, doi: 10.1016/j.rse.2013.03.002.

[17] M. Liu, X. Liu, J. Li, C. Ding, and J. Jiang, "Evaluating total inorganic nitrogen in coastal waters through fusion of multi-temporal RADARSAT-2 and optical imagery using random forest algorithm," *Int. J. Appl. Earth Observ. Geoinf.*, vol. 33, pp. 192–202, Dec. 2014, doi: 10.1016/j.jag.2014.05.009.

[18] X. Yu, S. Chen, and F. Chai, "Remote estimation of sea surface nitrate in the California current system from satellite ocean color measurements," *IEEE Trans. Geosci. Remote Sens.*, vol. 60, 2022, Art. no. 4203017, doi: 10.1109/TGRS.2021.3095099.

[19] X. Yuan et al., "Spatiotemporal dynamics and anthropologically dominated drivers of chlorophyll—A, TN and TP concentrations in the Pearl River Estuary based on retrieval algorithm and random forest regression," *Environ. Res.*, vol. 215, Dec. 2022, Art. no. 114380, doi: 10.1016/j.envres.2022.114380.

[20] T. Hou, W. Sun, C. Chen, G. Yang, X. Meng, and J. Peng, "Marine floating raft aquaculture extraction of hyperspectral remote sensing images based decision tree algorithm," *Int. J. Appl. Earth Observ. Geoinf.*, vol. 111, Jul. 2022, Art. no. 102846, doi: 10.1016/j.jag.2022.102846.

[21] J. Wang, Z. Wang, Y. Cui, and S. Yan, "Dynamic monitoring of phycocyanin concentration in Chaohu Lake of China using Sentinel-3 images and its indication of cyanobacterial blooms," *Ecolog. Indicators*, vol. 143, Oct. 2022, Art. no. 109340, doi: 10.1016/j.ecolind.2022.109340.

[22] P. Filippucci, L. Brocca, S. Bonafoni, C. Saltalippi, W. Wagner, and A. Tarpanelli, "Sentinel-2 high-resolution data for river discharge monitoring," *Remote Sens. Environ.*, vol. 281, Nov. 2022, Art. no. 113255, doi: 10.1016/j.rse.2022.113255.

[23] A. Morel and L. Prieur, "Analysis of variations in ocean color1," *Limnology Oceanogr.*, vol. 22, no. 4, pp. 709–722, Jul. 1977, doi: 10.4319/lo.1977.22.4.0709.

[24] E. Chraibi, F. de Boissieu, N. Barbier, S. Luque, and J.-B. Féret, "Stability in time and consistency between atmospheric corrections: Assessing the reliability of Sentinel-2 products for biodiversity monitoring in tropical forests," *Int. J. Appl. Earth Observ. Geoinf.*, vol. 112, Aug. 2022, Art. no. 102884, doi: 10.1016/j.jag.2022.102884.

[25] J. S. Dramsch, "70 years of machine learning in geoscience in review," in *Advances in Geophysics*, vol. 61, B. Moseley and L. Krischer, Eds. Amsterdam, The Netherlands: Elsevier, 2020, pp. 1–55.

[26] W. W. Hsieh, *Machine Learning Methods in the Environmental Science*. Cambridge, U.K.: Cambridge Univ. Press, 2009.

[27] L. Deng et al., "Retrieving phytoplankton size class from the absorption coefficient and chlorophyll a concentration based on support vector machine," *Remote Sens.*, vol. 11, no. 9, p. 1054, May 2019, doi: 10.3390/rs11091054.

[28] H. Ye, C. Yang, S. Tang, and C. Chen, "The phytoplankton variability in the Pearl River Estuary based on VIIRS imagery," *Continental Shelf Res.*, vol. 207, Dec. 2020, Art. no. 104228, doi: 10.1016/j.csr.2020.104228.

[29] M. Ashphaq, P. K. Srivastava, and D. Mitra, "Preliminary examination of influence of chlorophyll, total suspended material, and turbidity on satellite derived-bathymetry estimation in coastal turbid water," *Regional Stud. Mar. Sci.*, vol. 62, Sep. 2023, Art. no. 102920, doi: 10.1016/j.rsma.2023.102920.

[30] M. Zhu et al., "A review of the application of machine learning in water quality evaluation," *Eco-Environ. Health*, vol. 1, no. 2, pp. 107–116, Jun. 2022, doi: 10.1016/j.eehl.2022.06.001.

[31] Z. Liang, W. Wang, L. Liu, G. Li, and B. Xia, "Influence of commercial-scale seaweed cultivation on water quality: A case study in a typical laver culture area of the Yellow Sea, North China," *J. Mar. Sci. Eng.*, vol. 10, no. 5, p. 681, May 2022, doi: 10.3390/jmse10050681.

[32] M. D. Streicher, H. Reiss, and K. Reiss, "Impact of aquaculture and agriculture nutrient sources on macroalgae in a bioassay study," *Mar. Pollut. Bull.*, vol. 173, Dec. 2021, Art. no. 113025, doi: 10.1016/j.marpolbul.2021.113025.

[33] Y. Liu et al., "Satellite-based monitoring and statistics for raft and cage aquaculture in China's offshore waters," *Int. J. Appl. Earth Observ. Geoinf.*, vol. 91, Sep. 2020, Art. no. 102118, doi: 10.1016/j.jag.2020.102118.

[34] H. Jansen et al., "Spatio-temporal dynamics in the dissolved nutrient waste plume from Norwegian salmon cage aquaculture," *Aquaculture Environ. Interact.*, vol. 10, pp. 385–399, Sep. 2018, doi: 10.3354/aei00276.

Jingjing Huang received the B.S. degree in marine technology from the Nanjing University of Information Science and Technology, Nanjing, China, in 2019, and the M.S. degree in physical oceanography from the Second Institute of Oceanography, Ministry of Natural Resources, Hangzhou, China, in 2022. She is currently pursuing the Ph.D. degree with the Ocean College, Zhejiang University, Zhoushan, China.

Her research interests include the estimation of nutrient concentrations in offshore water with remote sensing technology.

Difeng Wang received the B.S. degree in electronic engineering from Xiamen University, Xiamen, China, in 2001, the M.S. degree in physical oceanography from the Second Institute of Oceanography, State Oceanic Administration, Hangzhou, China, in 2004, and the Ph.D. degree in electromagnetic fields and microwave techniques from the Graduate School of Chinese Academy of Sciences, Shanghai, China, in 2010.

He is currently a Research Scientist in remote sensing with the State Key Laboratory of Satellite Ocean Environment Dynamics, Second Institute of Oceanography. His research interests include ocean environment and water quality monitoring via satellites, including chlorophyll, nutrients, and suspended sediment in the open ocean and near shore waters.

Shuping Pan received the B.S. degree from the Shandong University of Science and Technology, Qingdao, China, in 1999, and the M.S. degree from Zhejiang University, Hangzhou, China, in 2002, both in Earth sciences.

She is currently a Senior Engineer with the Zhejiang Ecological Environment Monitoring Center, Hangzhou. Her research interests mainly focus on environmental monitoring and assessment, especially in the field of water environment monitoring.

Hongzhe Li received the B.E. degree in geomatics engineering from the School of Geodesy and Geomatics, Wuhan University, Wuhan, China, in 2021. He is currently pursuing the M.A. degree with the School of Oceanography, Shanghai Jiao Tong University, Shanghai, China.

His research interests include the processing of coastal zone remote-sensing images.
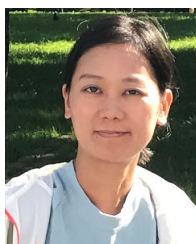
Fang Gong received the B.S. degree in computer and application from the Nanjing University of Information Science and Technology, Nanjing, China, in 2001.

She is currently a Senior Engineer with the State Key Laboratory of Satellite Ocean Environment Dynamics (SOED), Second Institute of Oceanography (SIO), Ministry of Natural Resources (MNR), Hangzhou, China. Her research interests include satellite data processing and analysis for ocean environment monitoring in the open ocean and near shore waters.

Haoyan Hu received the B.S. degree in marine biology from the Ocean University of China, Qingdao, China, in 1988.

He is currently a Professor-Level Senior Engineer with the Zhejiang Marine Ecology and Environment Monitoring Center, Zhoushan, China. His research interests include marine ecological environment monitoring and research.

Xianqiang He received the B.S. degree in marine and ocean engineering from the Huazhong University of Science and Technology, Wuhan, China, in 1999, the M.S. degree in physical oceanography from the Second Institute of Oceanography, Ministry of Natural Resources, Hangzhou, China, in 2002, and the Ph.D. degree in physical electronics from the Shanghai Institute of Technical Physics, Chinese Academy of Sciences, Shanghai, China, in 2007.

He is currently with the State Key Laboratory of Satellite Ocean Environment Dynamics, Second Institute of Oceanography, Ministry of Natural Resources, also with the Donghai Laboratory, Zhoushan, China, and the School of Oceanography, Shanghai Jiao Tong University, Shanghai. His research interests include radiative transfer in the coupled ocean and atmosphere system, atmospheric correction of satellite ocean color remote sensing, and oceanography research using ocean color remote sensing data.

Yan Bai received the B.S. and M.S. degrees from Sun Yat-sen University, Guangzhou, China, in 2000 and 2003, respectively, and the Ph.D. degree in electromagnetic fields and microwave techniques from the Shanghai Institute of Technical Physics, Chinese Academy of Sciences, Shanghai, China, in 2007.

She is currently with the State Key Laboratory of Satellite Ocean Environment Dynamics, Second Institute of Oceanography, Ministry of Natural Resources, Hangzhou, China, also with the Southern Marine Science and Engineering Guangdong Laboratory, Guangzhou, and the School of Oceanography, Shanghai Jiao Tong University, Shanghai. Her research interests include satellite remote sensing of the marine carbon cycle.

Zhuoqi Zheng received the B.S. degree in marine technology from the Ocean University of China, Qingdao, China, in 2019, the M.S. degree in physical oceanography from the Second Institute of Oceanography, Ministry of Natural Resources, Hangzhou, China, in 2022. He is currently pursuing the Ph.D. degree with the Geography and Ocean Science College, Nanjing University, Nanjing, China.

His research interests include the evaluation of water quality in offshore water with remote sensing technology.